

## Article

# Catalytic Activity of Zn(II) Coordination Polymer Based on a Cyclotriphosphazene-Functionalized Ligand for Removal of Organic Dyes

Ayşen Orhan Erkovan<sup>1</sup>, Azam Seifi<sup>1,2</sup> , Burcu Topaloğlu Aksoy<sup>1</sup>, Yunus Zorlu<sup>1</sup>, Alireza Khataee<sup>3,4,\*</sup>  and Bünyemin Çoşut<sup>1,\*</sup>

<sup>1</sup> Department of Chemistry, Gebze Technical University, Gebze 41400, Turkey

<sup>2</sup> Department of Applied Chemistry, Faculty of Chemistry, University of Tabriz, Tabriz 51666-16471, Iran

<sup>3</sup> Department of Environmental Engineering, Faculty of Engineering, Gebze Technical University, Gebze 41400, Turkey

<sup>4</sup> Research Laboratory of Advanced Water and Wastewater Treatment Processes, Department of Applied Chemistry, Faculty of Chemistry, University of Tabriz, Tabriz 51666-16471, Iran

\* Correspondence: akhataee@gtu.edu.tr (A.K.); bcosut@gtu.edu.tr (B.Ç.); Tel.: +90-262-605-3099 (A.K.); +90-262-605-3015 (B.Ç.)

**Abstract:** The 3D Zn(II) coordination polymer  $\{[Zn_3(L)(4,4'\text{-bpy})]_n\}$  (GTU-3) was prepared with a novel hexapod-shaped molecular building block, hexakis(methyl-2-(4-phenoxyphenyl)acetatebenzene) cyclotriphosphazene ( $H_6L_1$ ) by solvothermal reaction in dimethylformamide (DMF). Zn(II) coordination polymer was characterized by FTIR, thermal analysis, SEM-EDX, BET, powder X-ray diffraction analysis, and single crystal X-ray diffraction techniques. GTU-3 consists of six crystallographically independent  $Zn^{2+}$  ions, two fully deprotonated cyclophosphazene-based ligands, and two 4,4'-bipyridines (4,4'-bpy). In the complex, the flexible multisite cyclotriphosphazene bridging ligand ( $H_6L$ ) was completely deprotonated. GTU-3 exhibited relatively good catalytic activity toward Rhodamine B (RhB) removal in aqueous solution. A 0.4 g/L amount of GTU-3 could degrade the 10 mg/L solution of RhB up to 76.5% in the presence of peroxymonosulfate (PMS) oxidant in 1 h. The kinetic studies showed that the degradation process followed pseudo-first-order kinetic. By extending the degradation time to 5 h, the degradation efficiency reached 95.3%. Under the same conditions, Methylene Blue (MB) and Acid Red 17 (AR17) dyes were degraded by 86.2% and 52.8%, respectively.

**Keywords:** coordination polymer; Zn(II) complex; catalytic degradation; dye removal; peroxymonosulfate (PMS)



**Citation:** Erkovan, A.O.; Seifi, A.; Aksoy, B.T.; Zorlu, Y.; Khataee, A.; Çoşut, B. Catalytic Activity of Zn(II) Coordination Polymer Based on a Cyclotriphosphazene-Functionalized Ligand for Removal of Organic Dyes. *Catalysts* **2023**, *13*, 756. <https://doi.org/10.3390/catal13040756>

Academic Editors: Viorica Pârulescu, Veronica Brătan and Daniela Negoescu

Received: 15 February 2023

Revised: 9 April 2023

Accepted: 12 April 2023

Published: 15 April 2023



**Copyright:** © 2023 by the authors. Licensee MDPI, Basel, Switzerland. This article is an open access article distributed under the terms and conditions of the Creative Commons Attribution (CC BY) license (<https://creativecommons.org/licenses/by/4.0/>).

## 1. Introduction

With the increase in environmental pollution and the decrease in available water resources, controlling water pollution has become increasingly critical in today's world, especially considering the amount of pollutants present in industrial wastewater. Many processes in the industry are associated with the mixing of dye molecules with wastewater. As such, treatment of wastewater containing dye molecules is an important issue that needs to be addressed in order to protect both water resources and the environment. It is possible to remove these types of dyes from water using the catalytic degradation of dyes [1]. Many industries use different colorant species, especially a cationic fluorescent dye, RhB. The interaction between active media or pollutants and catalyst surfaces is important for the production of active species and the degradation of pollutants. It is critical to note that heterogeneous activation is strongly influenced by catalyst properties, especially surface characteristics. In the course of catalytic reactions, the surface characteristics of catalysts are crucial due to the solid–liquid contact near the catalyst's surface where the catalytic reactions often take place. Since coordination polymers have very high porosity and surface area, they have attracted considerable attention in the catalyst area. They are an excellent

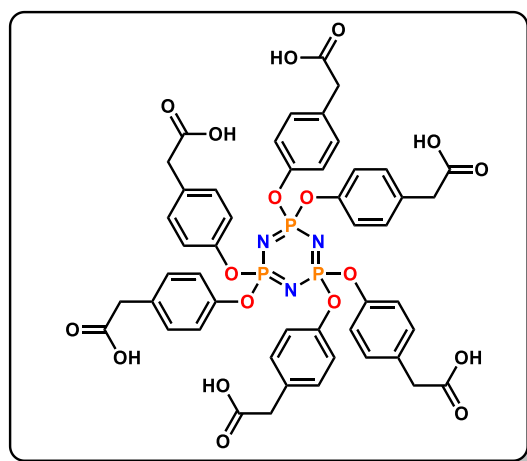
alternative to traditional catalysis since they bring together inorganic and organic matters at the same time [2].

Coordination polymers are inorganic/organic hydride structures built up by metal cation centers linked by organic building blocks. As early as the 1960s, it was synthesized for the first time [3,4]. There are coordination polymers that are capable of being coordinated and covalently connected in one, two, and even three dimensions. A one-dimensional chain can be formed when weak interactions exist, as well as a two-dimensional structure and a three-dimensional structure that arise from the interconnection of long bridge ligands. The advancement of technology over the past two decades has contributed to improving X-ray analysis devices and computer programs used in crystal structure analysis. The crystal engineering approach has benefited many researchers by enabling them to obtain coordination polymers with new topologies [5]. As a result, a larger number of coordination polymers have been obtained.

There is significant interest in this concept, since coordination polymers are capable of a wide range of applications, demonstrating their versatility. As a result of different metals and binder types being used to manufacture this material, it is capable of demonstrating a wide range of properties, such as gas storage, catalysis, magnetism, and fluorescence [6–11]. It has become increasingly imperative to construct coordination polymers based on flexible carboxylic ligands in recent years [12–15]. A carboxylic acid is an excellent tool to synthesize robust coordination polymers, in terms of both ensuring charge balance and bridging in a number of different ways.

There are many different coordination polymers used as catalyst candidates for the degradation of dyes in wastewater treatment. The role of the metal center is an important issue for designing the coordination polymers and tuning their catalytic efficiency. In this respect, Zn(II) is considered an appropriate metal for making these coordination polymers because its  $d^{10}$  configuration offers flexible stereochemistry. As a result, the geometries of the complexes can be easily changed, ranging from a tetrahedral geometry to square pyramidal and trigonal bipyramidal geometries to an octahedral geometry with varying degrees of distortion [16]. Because of the significant Lewis acid activity observed, this ion has been utilized in a number of catalytic processes [17]. Zn(II) complexes are easily able to take on a variety of 1D, 2D, and 3D configurations, but these also depend on the molar ratio, reaction conditions, the nature of the ancillary ligand, and coordinative skills.

For the preparation of coordination polymer, cyclophosphazenes which are an important part of inorganic cyclic systems were chosen as the core of synthesized hexacarboxylate organic ligand. As a result of the fact that phosphazenes can form coordination compounds with transition metals in recent years, more and more research is being conducted on this group of compounds. There are, however, few coordination polymers that contain cyclotriphosphazene-based ligands. Our group has utilized the flexible hexa-carboxylate ligand hexakis(methyl-2-(4-phenoxyphenyl)acetatebenzene) cyclotriphosphazene ( $H_6L_1$ , Scheme 1) in constructing a novel coordination polymer with transitional metal ions. In this work, we synthesize a newly designed coordination polymer based on Zn(II) metal centers, called GTU-3, and investigate its catalytic activity, one of the most frequently studied properties of coordination polymers. The catalytic activity of these structures has been tested by examining RhB degradation experiments, which has allowed us to investigate the catalytic activity of these structures. To make sure that the prepared structure can be applied as an efficient catalyst for dye degradation, another cationic dye, MB, and an anionic dye, AR17, were degraded by GTU-3. As part of the investigation of the degradation process, the effect of PMS oxidant on the process was also investigated [18]. Advanced oxidation processes (AOPs) are promising technologies that generate hydroxyl and sulfate radicals for pollutant degradation. Recently, much emphasis has been placed on the production of sulfate radicals via the activation of PMS. Because of its high reactivity and potential for generating sulfate radicals, PMS has gained popularity in recent years. In fact, it is becoming a viable substitute for hydrogen peroxide and persulfate. PMS is an unsymmetrical oxidant that can produce both hydroxyl and sulfate radicals when activated [19].



**Scheme 1.** Synthesized ligand ( $H_6L_1$ ) used to synthesize the Zn(II) coordination polymer.

## 2. Results and Discussions

### 2.1. Synthesis and Structural Characterization

Solvothermal conditions were used for GTU-3 synthesis, so a mixture of  $ZnCl_2$  and  $H_6L_1$ , whose chemical structure is given in Scheme 1 with a molar ratio of 4:1, was heated at  $80\text{ }^\circ\text{C}$  for one day. Both synthesis processes resulted in needle-like colorless crystals. According to the IR spectra of  $H_6L_1$  and GTU-3 shown in Figure 1, some characteristic absorption bands can be seen, which are mostly related to the asymmetric (*vas*: ca.  $1638\text{ cm}^{-1}$ ) and symmetric (*vs*: ca.  $1398\text{ cm}^{-1}$ ) stretching vibrations of the carboxylate groups. The sharp peaks that appear at  $1161\text{ cm}^{-1}$  in the FTIR spectra of  $H_6L_1$  correspond to stretching vibrations of the P=N groups. The increase in Zn metal clusters in coordination polymers slightly decreased the frequency of P=N stretching. The strong band at  $958\text{ cm}^{-1}$  is assigned to P-O stretching in the experimental IR spectrum of the GTU-3, and  $H_6L_1$ . The presence of no bands in the region  $1690\text{--}1730\text{ cm}^{-1}$  indicates complete deprotonation of the carboxylate groups and is consistent with the result of the single crystal X-ray diffraction analysis.

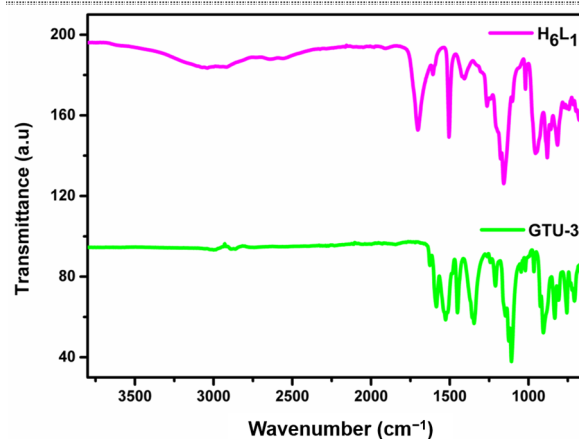


**Figure 1.** FTIR spectrum of the synthesized GTU-3 and  $H_6L_1$ .

Morphological clarification was achieved by SEM analysis, and the obtained images of GTU-3 are given in Figure 2. The images show rod-shaped particles and a layered structure. For the chemical characterization and elemental analysis of the GTU-3, EDX analysis was performed, and the results are given in Figure 3. As the obtained results, elemental composition of synthesized GTU-3 are consistent with the expected percentages. The high presence of Zn atoms in the elemental percentages supports successful synthesis.

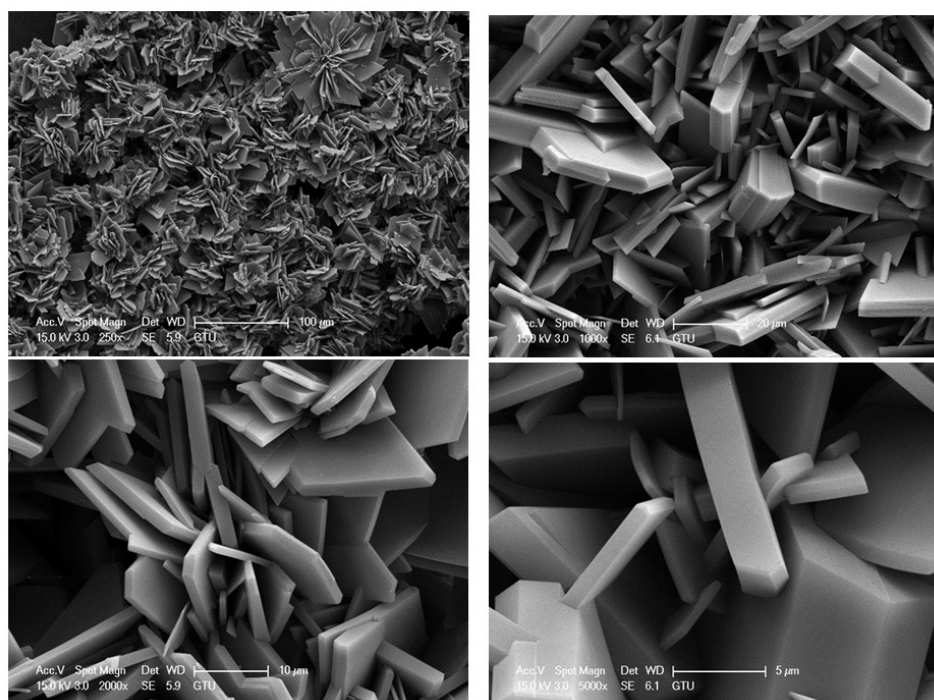


Figure 2. SEM images of the GTU-3.

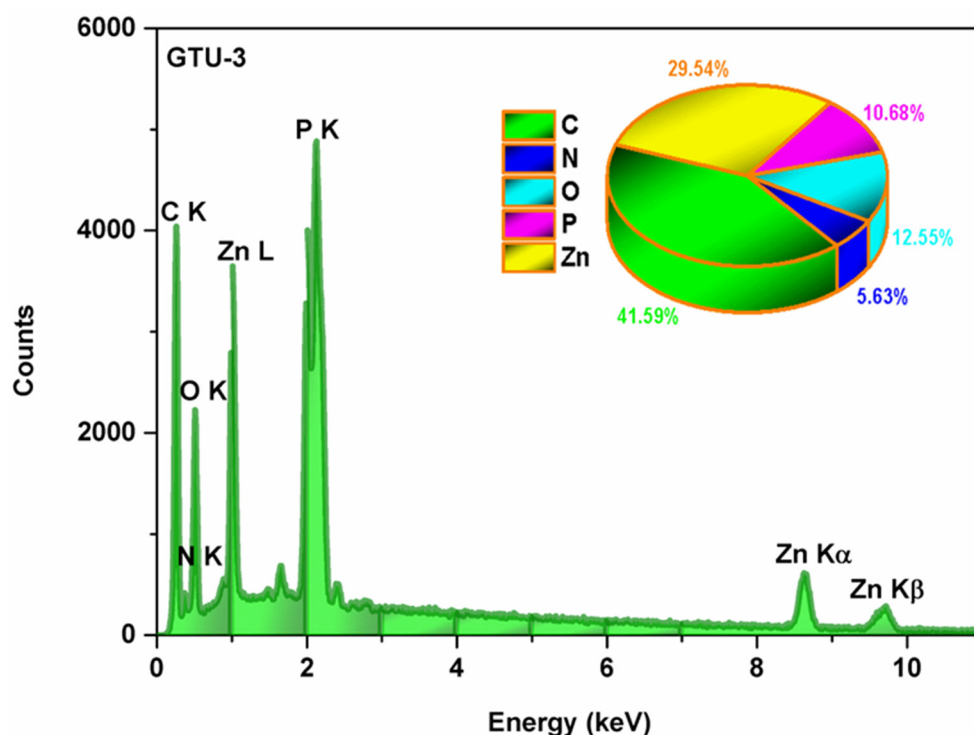
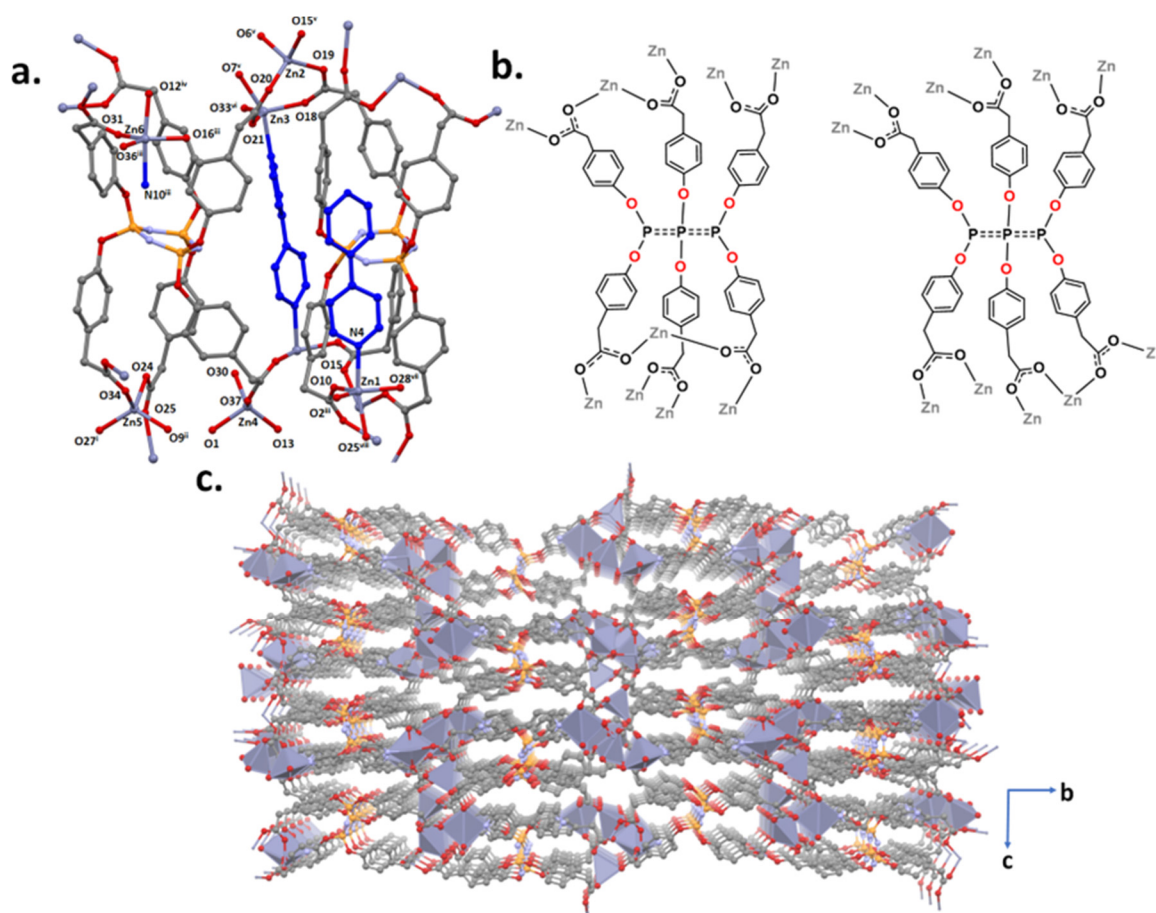


Figure 3. EDX spectra of the GTU-3.

## 2.2. Description of Crystal Structures

The reaction of  $\text{ZnCl}_2$  with  $\text{H}_6\text{L}_1$  under conventional conditions at  $80\text{ }^\circ\text{C}$  resulted in a 3D coordination polymer, namely  $\{[\text{Zn}_6(\text{L})_2(4,4'\text{-bpy})_2]\}_n$ . The asymmetric unit of GTU-3 consists of six crystallographically independent  $\text{Zn}^{2+}$  ions, two fully deprotonated cyclophosphazene-based ligands, and two 4,4'-Bipyridine (4,4'-bpy) (Figure 4a). GTU-3 crystallizes in the monoclinic crystal system with  $P2_1/n$  space group. Regarding the hexacarboxylated cyclophosphazene ligands, three of the six-carboxylate arms are situated

above the central heterocyclic ring, and the other three below. Zn1 and Zn6 central atoms have similar coordination environments and are distorted square pyramidal coordination geometry composed of four carboxylate oxygen atoms (O2, O10, O25, O28 for Zn1; O12, O15, O31, O36 for Zn2) and one nitrogen atom of 4,4'-bpy (N4 for Zn1; N10 for Zn6). Zn2, Zn4, and Zn5 ions are four-coordinate through four carboxylate oxygen atoms to give distorted tetrahedral coordination geometry. Zn3 ion is a distorted tetrahedral geometry by three carboxylate oxygen atoms and one nitrogen atom of 4,4'-bpy. The Zn-O<sub>carboxylate</sub> bond distance is in the range of 1.919 (5) Å–2.136 (6) Å, comparable to reported bond lengths in other N<sub>3</sub>P<sub>3</sub>-based hexacarboxylated Zn complexes [20]. As indicated in Figure 4b, there are two fully deprotonated cyclophosphazene-based linkers with different coordination modes in the crystal structure. The one cyclophosphazene linker adopts a  $\mu_{10}$  coordination binding mode, in which carboxylate groups have three syn-syn- $\mu_2$ - $\eta^1$ : $\eta^1$  and three syn-anti- $\mu_2$ - $\eta^1$ : $\eta^1$  binding modes, while the other linker in the asymmetric unit has a  $\mu_{11}$  coordination binding mode involving five syn-syn- $\mu_2$ - $\eta^1$ : $\eta^1$  and one syn-anti- $\mu_2$ - $\eta^1$ : $\eta^1$  coordination mode (Figure 4b). On the other hand, the nitrogen atom in one of the two bipyridine ligands does not participate in coordination. In Figure 4c, an image of three-dimensional coordination polymer by a-axis is shown. The P-N distances in GTU-3 are typically in the range of 1.565 (6) Å–1.598 (6) Å and the average N-P-N and P-N-P angles are 117.25° and 121.65° [21,22].



**Figure 4.** (a) Ball-stick representation of crystal structure of GTU-3. All H-atoms were omitted for clarity, and 4,4'-bpy units are shown in blue. (b) Coordination modes of deprotonated ligand (L). (c) View of three-dimensional coordination polymer looking down the a-axis. Symmetry transformations used to generate equivalent atoms: (i): 1.5-x,-1/2+y,1/2-z; (ii): 1-x,1-y,1-z; (iii): -1/2+x,1.5-y,-1/2+z; (iv): 1-x,2-y,1-z; (v): 1.5-x,1/2+y,1.5-z; (vi): 1/2+x,1.5-y,1/2+z; (vii): -1/2+x,1.5-y,1/2+z; (viii): 1-x,1-y,1-z.

### 2.3. Powder Diffraction, Thermal Properties, and Gas Sorption Measurement

In order to confirm the bulk phase purity of GTU-3, powder X-ray diffraction analyses were performed. As shown in Figure 5a, experimental PXRD pattern diffraction peaks are almost matched with the simulated pattern (CIF), indicating that the as-synthesized coordination polymers are undoubtedly GTU-3.

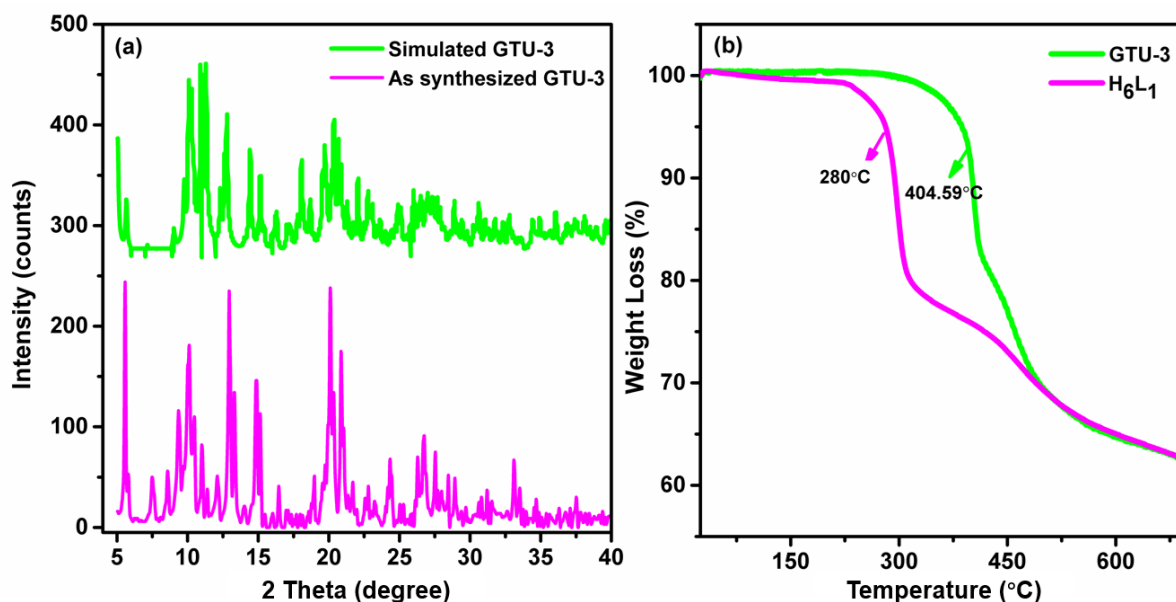


**Figure 5.** (a) Simulated and experimental PXRD patterns of GTU-3, (b) TGA thermogram of the synthesized GTU-3 and H<sub>6</sub>L<sub>1</sub>.

Thermogravimetric analysis (TGA) was performed for single crystalline samples of H<sub>6</sub>L<sub>1</sub>, GTU-3 under N<sub>2</sub> atmosphere while the heating rate was 10 K/min, and the results are given in Figure 5b. The TG curve of H<sub>6</sub>L<sub>1</sub> remains unimpaired until 280 °C. Then, the coordination polymer remains undamaged until 404.59 °C and then starts to break down (obsd: 37.7%). The zinc-based coordinations' polymers appear to have high thermo-stability, which is due to the stable hexa-carboxylate ligands.

### 2.4. Catalytic Efficiency of the Prepared GTU-3

As mentioned above, the synthesized coordination polymer can act as a catalyst. In the present study, we applied its catalytic potential for dye degradation. At RT, magnetic stirring was used in every experiment involving catalytic degradation. First of all, some preliminary experiments were performed to find the appropriate ranges of the effective parameters on degradation efficiency, including the initial concentration of the dye solution, PMS amount, and degradation time. Then, the degradation tests were performed at different conditions, namely, in the presence of bare GTU-3, bare PMS, and both of them at the same time. The effect of catalyst amount on RhB degradation efficiency was also surveyed. The observed results showed that the optimum amount of GTU-3 was found to be 0.40 g/L, as shown in Figure S1 (in the Supplementary Materials). According to the results shown in Figure 6, by using bare GTU-3, the degradation efficiency is not so impressive, by using bare PMS, DE% increases to 23%, while introducing both GTU-3 and PMS to the dye solution increases the degradation efficiency dramatically, up to ~76% (Figure 6a). It can be due to the synergistic effect between GTU-3 and PMS. Furthermore; absorption spectra of RhB degradation in the presence of GTU-3 and PMS are given in Figure S2 (in the Supplementary Materials).

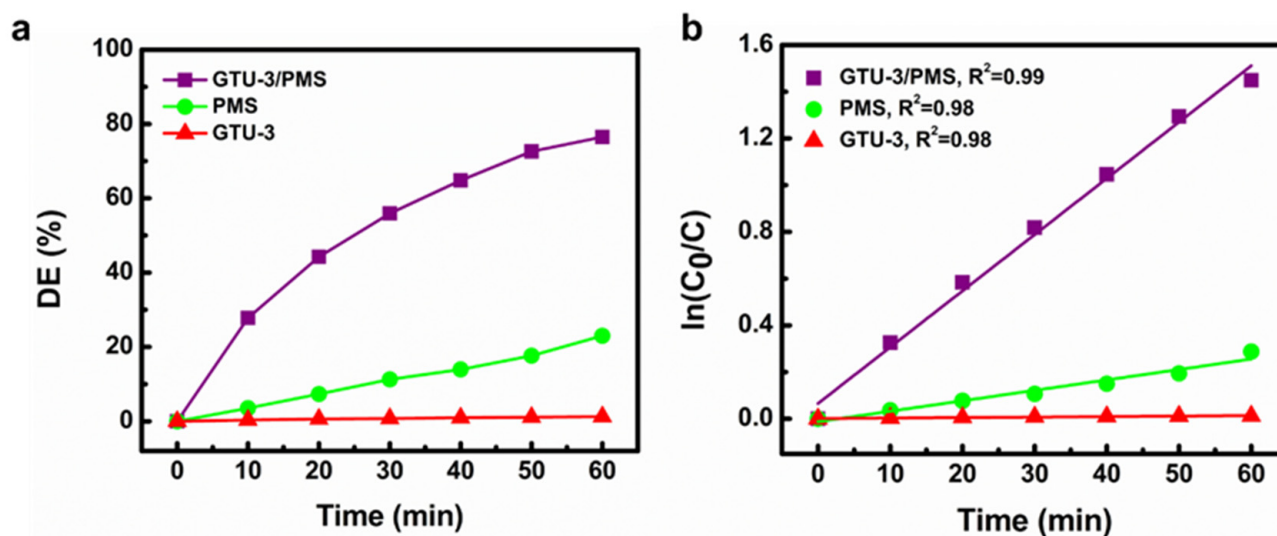


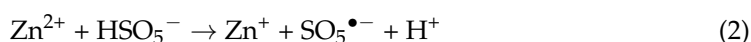
**Figure 6.** (a) Catalytic degradation efficiency of GTU-3 at different conditions,  $[\text{RhB}]_0 = 10 \text{ mg/L}$  (50 mL),  $[\text{PMS}] = 0.5 \text{ mM}$ ,  $\text{GTU-3} = 0.4 \text{ g/L}$ , and (b) pseudo-first-order kinetic model graph for the processes in plot a.

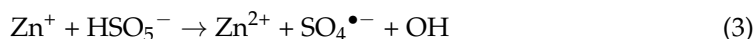
It was assumed that the degradation process obeyed pseudo-first-order kinetics, and the  $\ln(C_0/C)$  graph was plotted versus time (Figure 6b). The linear plots with high  $R^2$  values proved this assumption to be true. Therefore, the slope of the obtained trendline could be considered as the reaction  $k_{\text{app}}$ . Applying this  $k_{\text{app}}$ , the synergistic effect (SE) between the simultaneous presence of GTU-3 and PMS could be calculated using the following equation (Equation (1)) [23]:

$$\text{SE}\% = \frac{[k_{\text{app,combined process}} - (k_{\text{app, process 1}} + k_{\text{app, process 2}})]}{k_{\text{app,combined process}}} \times 100 \quad (1)$$

$\text{SE} > 0$  means that the two factors involved in the process have a reinforcing effect on each other. According to Figure 6b, the  $k_{\text{app}}$  values were  $0.0256 \text{ min}^{-1}$ ,  $0.0042 \text{ min}^{-1}$  and  $0.0002 \text{ min}^{-1}$  for the degradation processes performed in the presence of GTU-3 and PMS, bare PMS, and bare GTU-3, respectively. Therefore, the SE% was calculated to be 82.8%, which proves the enhancing effect of GTU-3 and PMS in the presence of each other.

The Lewis acid site of the surface is involved in the catalytic oxidation of metal oxides. Abundant  $\text{H}_2\text{O}$  molecules are adsorbed to the surface of the metal oxide catalyst when it is added to an aqueous solution. Water molecules split apart to form  $\text{OH}^-$  and  $\text{H}^+$ , which combine with surface metal atoms and oxygen-containing sites, respectively, to form surface hydroxyl groups. The metal oxide's hydroxyl group is visible as a Bronsted acid point. Unsaturated covalent oxygen atoms and metal cations exhibit Lewis acid and Lewis basic points, respectively [24]. In addition, it is assumed that RhB degradation occurs via two parallel mechanisms, radical and nonradical mechanisms [25]. The longer  $\text{M} \dots \text{O}$  bond can be considered a weak coordination bond [26]. The weak carboxylate  $\text{M} \dots \text{O}$  coordination with the corresponding metal center can act as an active Lewis acid site. For GTU-3, the carboxylate bond lengths were measured as  $2.136 \text{ \AA}$  ( $\text{Zn1} \dots \text{O25iv}$ ), which supports the weak carboxylate bonding. Consequently, the metal core and weak carboxylate coordinations can act as active Lewis acid centers with the potential to initiate a catalytic reaction by attacking the PMS oxidant molecule from the O end. This process can lead to the production of  $\text{SO}_4^{\bullet-}$  radicals according to the following reactions (Equations (2) and (3)), which consequently starts the radical process [27].





The produced  $\text{SO}_4^{\bullet-}$  radicals attack the RhB molecules and initiate the degradation process.

According to the obtained results, GTU-3 showed good catalytic activity. This may be due to the 4,4-bpy ligands bound to the Zn core in the structure of the prepared GTU-3 coordination polymers. In the non-radical process, the product of the radical reaction, the  $\text{H}^+$  ion, increases the acidity of the already acidic reaction medium. These protons can increase the removal efficiency of GTU-3. They can quaternize the open-ended N atom of the 4,4-bpy groups attached to GTU-3 and make a complex with PMS and then react with the adsorbed RhB molecules, as shown in Figure 7. As a result, degradation can occur. This interaction also significantly increases the catalytic performance of GTU-3 [28]. Figure 6 shows that this increase in catalytic efficiency is due to the presence of acidic protons. As can be seen in Figure 8, the same reactions were performed in the basic medium, and according to the results, the catalytic efficiency decreased due to the decreased acidic protons in the basic medium. It is worth mentioning that the band gap value of GTU-3 was obtained 3.79 eV from the reflection data (Figure S3, in the Supplementary Materials).

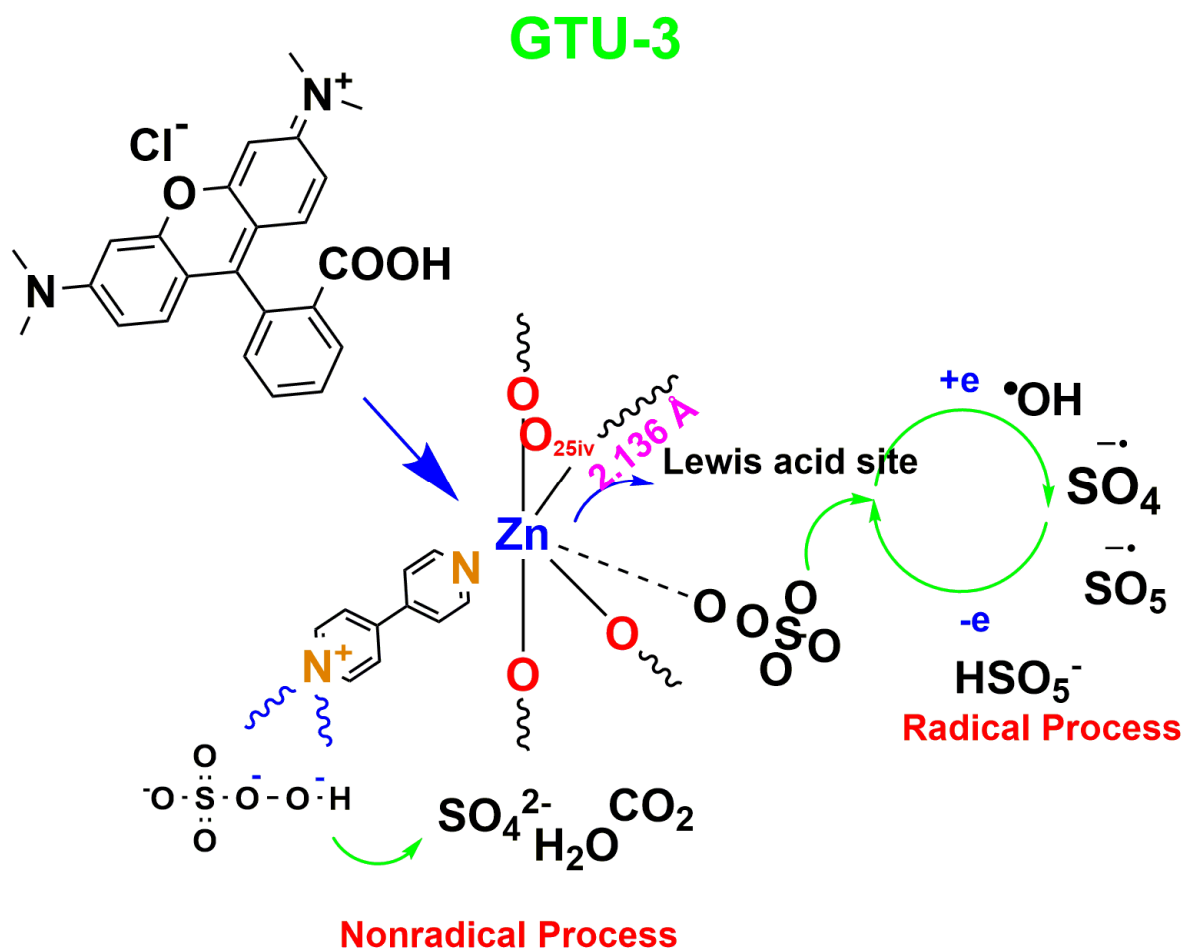
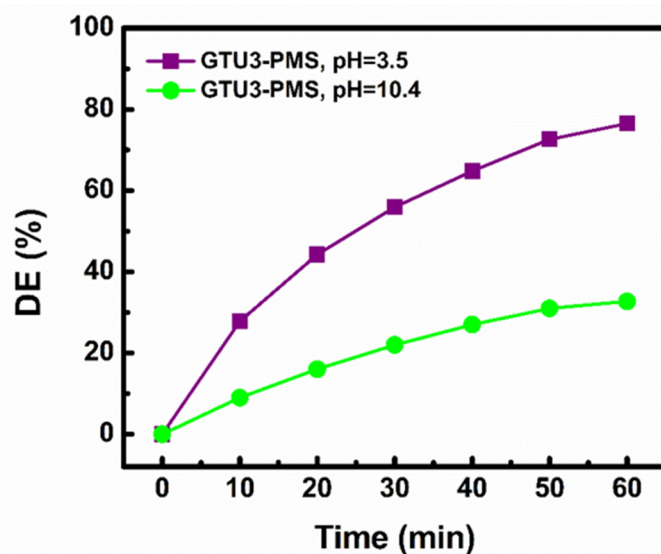
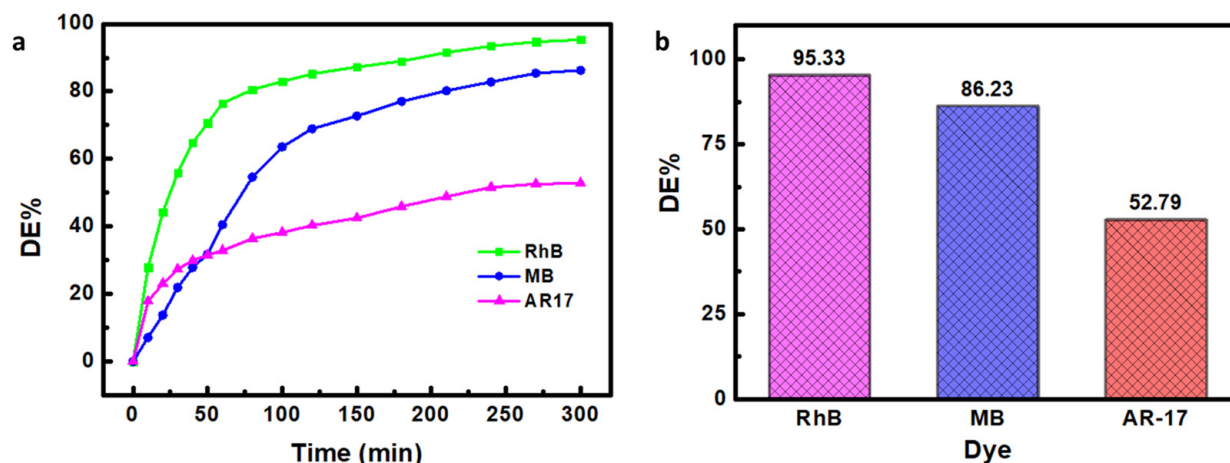


Figure 7. The radical and nonradical PMS activation process in the presence of GTU-3.



**Figure 8.** Catalytic degradation efficiency of GTU-3 at pH = 10.4,  $[RhB]_0 = 10$  mg/L (50 mL),  $[PMS] = 0.5$  mM, and GTU-3 = 0.4 g/L.

As mentioned above, the degradation of 76% was obtained after 1 h. The degradation time was extended to 5 h to pursue the degradation trend for longer times. It was shown that after 5 h, the DE% reached 95.3% (Figure 9a). Under the same conditions, the degradation of cationic MB and anionic AR17 was also investigated. According to the results, MB and AR17 were degraded by 86.2% and 52.8% after 5 h. Figure 9a,b show the comparison of DE% for different dyes. The successful removal of both anionic and cationic dyes by GTU-3 proves its high potential as an efficient catalyst for different dyes' degradation. However, it seems that GTU-3 has better activity for the degradation of cationic dyes.



**Figure 9.** (a) Catalytic degradation efficiency of GTU-3 at the dye initial concentration of 10 mg/L (50 mL),  $[PMS] = 0.5$  mM, and GTU-3 = 0.4 g/L, and (b) the bar graph of the dyes degradation.

### 3. Materials and Methods

#### 3.1. Materials

Methyl 4-hydroxyphenyl acetate (Sigma-Aldrich, St. Louis, MO, USA), anhydrous potassium carbonate  $\geq 99.0\%$  Sigma-Aldrich, St. Louis, MO, USA), anhydrous acetone (Aldrich, St. Louis, MO, USA  $\geq 99.0\%$ ), phosphonitrilic chloride (Alfa Easer, Ward Hill, Massachusetts, USA 98%), DCM (Merck, Darmstadt, Germany),  $NaSO_4$  (Merck, Darmstadt, Germany), THF (Sigma-Aldrich, St. Louis, MO, USA), hexane (Merck, Darmstadt, Germany), sodium hydroxide (Merck, Darmstadt, Germany), methanol (Merck, Darmstadt,

Germany), hydrochloric acid (Sigma-Aldrich, St. Louis, MO, USA),  $\text{Zn}(\text{Cl})_2$  (Fluka AG, Buchs, Switzerland), DMF (Merck, Darmstadt, Germany), Rhodamine B (Sigma St. Louis, MO, USA), potassium monopersulfate (Merck, Darmstadt, Germany), methylene blue (Sigma-Aldrich, St. Louis, MO, USA), acidic red-17 (Sigma-Aldrich, St. Louis, MO, USA).

### 3.2. Synthesis

#### 3.2.1. Synthesis of Hexakis(methyl-2-(4-phenoxyphenyl)acetate)benzene Cyclotriphosphazene ( $\text{H}_6\text{L}_1$ )

Anhydrous potassium carbonate (2.77 g, 20.09 mmol) was poured into an anhydrous acetone (50 mL) solution, which contained methyl 4-hydroxyphenylacetate (3.3 g, 20.09 mmol) and phosphonitrilic chloride trimer  $\text{N}_3\text{P}_3\text{Cl}_6$  (1.00 g, 2.87 mmol) and was heated in reflux conditions for 36 h while being stirred constantly under an argon atmosphere. The reaction solvent was removed with a rotary evaporator after being cooled to room temperature. To extract the obtained solid compound, 50 mL of water and DCM was used. Then, anhydrous  $\text{Na}_2\text{SO}_4$  was added to dry the organic phase. For purifying the obtained unpurified product, it was passed through a silica gel chromatography column, with Hexane:THF (3:2) as the mobile phase. After drying the product ( $\text{N}_3\text{P}_3(\text{OC}_6\text{H}_4\text{CH}_3\text{COOCH}_3)_6$ ), a white powder (2.8 g, 80% yield based on  $\text{N}_3\text{P}_3\text{Cl}_6$ ) was obtained. MALDI-TOF ( $m/z$ ) Calc. 1125.26  $m/z$ , Found: 1126.078  $[\text{M} + \text{H}]^+$  (Figure S4, in the Supplementary Materials).  $^1\text{H-NMR}$  (400 MHz,  $\text{DMSO-d}_6$ , ppm), 7.10 (d, 12H, Ar-H), 6.88 (d, 12H, Ar-H), 3.69 (s, 2H,  $-\text{CH}_2$ ), 3.60 (s, 3H,  $-\text{CH}_3$ ) (Figure S5, in the Supplementary Materials).

A 0.77 g amount of sodium hydroxide (19 mmol) was dissolved in 50 mL of methanol, and then 1.35 g  $\text{N}_3\text{P}_3(\text{OC}_6\text{H}_4\text{CH}_3\text{COOCH}_3)_6$  (1.19 mmol) was added to the reaction mixture. The obtained mixture was heated up to 80 °C and was stirred overnight at this temperature. During this process, the volatile compounds were eliminated, and the rest were dissolved in water. Then, it was filtered, and its pH was set in the range of 2–3 using dilute hydrochloric acid. After stirring, the product precipitated, which was separated by filtering. Then, it was washed with water and then was dried (0.90 g, 72% yield). This step resulted in the pure isolation of  $\text{H}_6\text{L}_1$ . MALDI-TOF ( $m/z$ ) Calc. 1041.78  $m/z$ , Found: 1042.55  $[\text{M} + \text{H}]^+$  (Figure S6, in the Supplementary Materials).  $^1\text{H-NMR}$  (400 MHz,  $\text{DMSO-d}_6$ , ppm), 7.14 (d, 12H, Ar-H), 6.82 (d, 12H, Ar-H), 3.55 (s, 12H,  $-\text{CH}_2$ ) (Figure S7, in the Supplementary Materials). IR  $\nu$  ( $\text{cm}^{-1}$ ): 2953 ( $-\text{C-H}$ ), 1734 ( $-\text{C=O}$ ), 1505 ( $-\text{C-O-}$ ), 1154 ( $-\text{P=N-}$ ), 956 ( $-\text{P-O-}$ ) for  $\text{N}_3\text{P}_3(\text{OC}_6\text{H}_4\text{CH}_3\text{COOCH}_3)_6$ , and 3039 ( $-\text{OH}$ ), 1702 ( $\text{C=O}$ ), 1606–1407 ( $\text{C=C}$ ), 1157 ( $-\text{P=N-}$ ), 951 ( $-\text{P-O-}$ ) for  $\text{H}_6\text{L}_1$  (Figure S8, in the Supplementary Materials).

#### 3.2.2. Synthesis of GTU-3

$\text{ZnCl}_2$  (2.6 mg, 19.2 mmol, and 4 mol) and  $\text{H}_6\text{L}_1$  (5 mg, 4.8 mmol, and 1 mol) were mixed and dissolved in 3 mL of DMF– $\text{H}_2\text{O}$  (2:1,  $v/v$ ). After sealing the obtained solution in a 4 mL glass bottle, it was heated up to 80 °C and kept at this temperature for 1 day to obtain colorless crystals. After synthesis, obtained crystals were washed with mother solvents several times and dried in an oven for 1 day. The structural characterizations of the synthesized GTU-3 were exhibited in the present manuscript.

### 3.3. X-ray Data Collection and Structure Refinement

Intensity data collection was carried out on a Bruker APEX II QUAZAR three-circle diffractometer. Indexing was performed using APEX2 [29]. Data integration and reduction were carried out with SAINT [30]. Absorption correction was performed using the multi-scan method implemented in SADABS [31]. The structure was solved using SHELXT [32] and then refined by full-matrix least-squares refinements on F2 using the SHELXL [33] in Olex2 Software Package (v.1.5, OlexSys, Regensburg, Germany) [34]. SQUEEZE [35] was also applied to remove electron density caused by highly disordered solvent molecules. The total potential solvent area for GTU-3 occupied 7.3% ( $856.00 \text{ \AA}^3/11,679.9 \text{ \AA}^3$ ). Analysis of solvent-accessible voids in the structure was performed using the CALC SOLV within the PLATON software package with a probe radius of 1.20 Å and grid spacing of 0.2 Å. Van der

Waals (or ion) radii used in the analysis are C (1.70 Å), H (1.20 Å), Zn (2.25 Å), N (1.55 Å), O (1.52 Å), and P (1.80 Å), respectively. The positions of all H-atoms bonded to carbon, nitrogen, and oxygen atoms were geometrically optimized with the following HFIX instructions in SHELXL: HFIX 23 for the  $-\text{CH}_2-$  moieties and HFIX 43 for the CH of the aromatic rings. Finally, their displacement parameters were set to isotropic thermal displacements parameters ( $U_{\text{iso}}(\text{H}) = 1.2 \times U_{\text{eq}}$  for CH and  $\text{CH}_2$  groups or  $U_{\text{iso}}(\text{H}) = 1.5 \times U_{\text{eq}}$  (-OH). One pyridyl ring in GTU-3 is disordered over two positions with occupancies of 0.74:0.26. Crystallographic data and refinement details of the data collection are given in Table 1. Crystal structure validations and geometrical calculations were performed using PLATON software [36]. Mercury software [37] was used for the visualization of the CIF file. Bond lengths and angles are given in Table S1. Additional crystallographic data with CCDC reference number 2075651 (GTU-3) were deposited within the Cambridge Crystallographic Data Center via [www.ccdc.cam.ac.uk/deposit](http://www.ccdc.cam.ac.uk/deposit) (accessed on 1 February 2023).

**Table 1.** Crystal data and structure refinement details for GTU-3.

CCDC	2075651
Formula of refinement model	$\text{C}_{116}\text{H}_{88}\text{N}_{10}\text{O}_{36}\text{P}_6\text{Zn}_6$
Formula weight (g/mol)	2776
Temperature (K)	296
Radiation, Wavelength (Å)	MoK $\alpha$ ( $\lambda = 0.71073$ )
Crystal system	Monoclinic
Space group	$P2_1/n$
a/Å	19.9651(12)
b/Å	32.5061(17)
c/Å	20.2465(11)
$\alpha/^\circ$	90
$\beta/^\circ$	117.265(3)
$\gamma/^\circ$	90
Crystal size/mm <sup>3</sup>	$0.27 \times 0.22 \times 0.051$
Volume/Å <sup>3</sup>	11,679.9(12)
Z	4
$\rho_{\text{calcd}}$ (g/cm <sup>-3</sup> )	1.579
$\mu$ (mm <sup>-1</sup> )	1.383
F(000)	5648
2 $\Theta$ range for data collection/ $^\circ$	2.506 to 50.054
Index ranges (h/k/l)	$-23 \leq h \leq 21, -38 \leq k \leq 38, -23 \leq l \leq 24$
Reflections collected	136,299
Independent reflections	20,528 [ $R_{\text{int}} = 0.2798, R_{\text{sigma}} = 0.2313$ ]
Data/restraints/parameters	20,528/114/1622
Goodness-of-fit on $F^2$ (S)	0.964
Final R indices [ $I > 2\sigma(I)$ ]	$R_1 = 0.0653, wR_2 = 0.0985$
R indices (all data)	$R_1 = 0.2230, wR_2 = 0.1379$
Largest diff. peak/hole/e Å <sup>-3</sup>	0.38/−0.40

### 3.4. Catalytic Dye Degradation

The catalytic activity of the obtained GTU-3 was investigated in a set of dye-degradation tests. RhB dye was selected as the model pollutant. For the degradation tests, 50 mL of 10 mg/L RhB solutions were poured into beakers, and then GTU-3 was added to the solutions. A known amount of PMS was also added when needed. The content of the beakers was stirred magnetically during the tests. The changes in concentration of the RhB solutions during the catalytic degradation were monitored at  $\lambda = 554$  nm using a UV-Vis spectrophotometer, Shimadzu, UV-2600. Sampling was performed with time intervals of 10 min starting from  $t = 0$ , and the degradation efficiency (DE%) was calculated. The degradation tests were conducted at room temperature and normal ambient pressure. To prove the efficiency of GTU-3 as a catalyst for the removal of other groups of dyes, the degrada-

tion of MB and AR17 dyes was investigated under the same conditions. The changes in concentration of these two dyes were followed at  $\lambda = 662$  and 532 nm, respectively.

### 3.5. Characterizations

$^1\text{H}$  and  $^{31}\text{P}$  NMR spectra for the ligand were recorded on a Varian INOVA 500 MHz spectrometer (Varian, Palo Alto, CA, USA). IR spectra were recorded between 4000 and 650  $\text{cm}^{-1}$  using a Perkin Elmer Spectrum 100 FT-IR spectrometer (Waltham, MA, USA) with an attenuated total reflection (ATR). Positive ion and linear mode MALDI-MS of HPCP was obtained in dihydroxybenzoic acid as the MALDI matrix using nitrogen laser accumulating 50 laser shots using a Bruker Microflex LT MALDI-TOF mass spectrometer (karlsruhe, Germany). Thermal gravimetric analyses (TGA) were carried out on a Mettler Toledo Stare Thermal Analysis System (Greifensee, Switzerland) at a heating rate of 10  $^\circ\text{C min}^{-1}$  over a temperature range of 25–900  $^\circ\text{C}$  under a nitrogen flow (50  $\text{mL min}^{-1}$ ). The surface morphology and energy dispersive X-ray analysis (EDX) were recorded with an FEI (PHILIPS) XL30 SFEG scanning electron microscope (SEM) (Amsterdam, the Netherlands). Powder X-ray diffraction (PXRD) measurements were carried out on a Bruker Advanced D8 X-ray diffractometer (karlsruhe, Germany) with  $\text{Cu K}\alpha$  ( $\lambda = 1.5405 \text{ \AA}$ ) radiation source operating at 30 kV and 30 mA. The patterns were recorded over the  $2\Theta$  range of 1–50 $^\circ$  with step size = 0.02 $^\circ$ .

## 4. Conclusions

Based on the findings of our study, we demonstrate that cyclotriphosphazene-functionalized scaffolds can be used to synthesize a novel molecular building block. A mild solvothermal reaction of the linker (L) with Zn(II) ions resulted in the formation of three-dimensional pillared layers of coordination polymers. When the same reaction conditions were used, merely adding 4,4-bpy as an ancillary ligand resulted in the formation of a 3D coordination polymer involving a zinc-carboxylate-based 1D inorganic building block. The catalytic activity of the coordination polymer obtained in this study was investigated using the RhB dye degradation process. To increase the activity of coordination polymers, PMS was added to the process. PMS is an excellent oxidant that can increase their activity. Although PMS is a strong oxidant in terms of thermodynamics, its direct reaction with the majority of pollutants is too slow, necessitating activation. With the production of protons, PMS can automatically adjust the pH of the solution. When activated, it produces sulfate radicals, which play an important role in pollutant degradation. Furthermore, the hydroxyl radical is a valuable byproduct of PMS activation. According to the results obtained in this study, GTU-3 exhibits significant catalytic activity. In terms of how dye is removed from GTU-3, it is thought that a mix of radical and non-radical mechanisms is involved. As a potential catalyst, GTU-3 has shown some promise in a variety of catalytic processes, based on the recorded research.

**Supplementary Materials:** The following supporting information can be downloaded at: <https://www.mdpi.com/article/10.3390/catal13040756/s1>, Figure S1: Catalytic degradation of RhB using GTU-3 along with PMS,  $[\text{RhB}]_0 = 10 \text{ ppm}$  (50 mL),  $[\text{PMS}] = 0.5 \text{ mM}$  at different catalyst concentrations; Figure S2: Absorption spectra of RhB degradation for GTU-3,  $[\text{RhB}]_0 = 10 \text{ ppm}$  (50 mL),  $[\text{PMS}] = 0.5 \text{ mM}$ , catalyst = 0.4 g/L; Figure S3: Band gap energy of GTU-3 calculated from the reflection data; Figure S4: MALDI MS Spectrum of  $\text{N}_3\text{P}_3(\text{OC}_6\text{H}_4\text{CH}_3\text{COOCH}_3)_6$ ; Figure S5:  $^1\text{H}$ -NMR spectra of compounds  $\text{N}_3\text{P}_3(\text{OC}_6\text{H}_4\text{CH}_3\text{COOCH}_3)_6$  in  $\text{DMSO-d}_6$ ; Figure S6: MALDI MS Spectrum of  $\text{H}_6\text{L}_1$ ; Figure S7:  $^1\text{H}$ -NMR spectra of compounds  $\text{H}_6\text{L}_1$  in  $\text{DMSO-d}_6$ ; Figure S8: FTIR spectrum of the synthesized  $\text{N}_3\text{P}_3(\text{OC}_6\text{H}_4\text{CH}_3\text{COOCH}_3)_6$  and  $\text{H}_6\text{L}_1$ ; Table S1: Selected bond lengths ( $\text{\AA}$ ) and bond angles ( $^\circ$ ) for GTU-3.

**Author Contributions:** Conceptualization, B.Ç.; investigation, A.O.E., A.S.; project administration, B.Ç., Y.Z., A.K.; resources, B.Ç., Y.Z., A.K.; supervision, B.Ç.; validation, B.Ç., Y.Z., A.K.; writing—original draft, A.O.E., A.S., B.T.A., Y.Z.; writing—review and editing, B.Ç., A.K. All authors have read and agreed to the published version of the manuscript.

**Funding:** This research was funded by GTU (Gebze Technical University) grant number G.T.Ü. BAP 2021-A-102-02.

**Data Availability Statement:** Not applicable.

**Conflicts of Interest:** There are no conflicts of interest to declare.

## References

1. Kohantorabi, M.; Hosseinifard, M.; Kazemzadeh, A. Catalytic activity of a magnetic Fe<sub>2</sub>O<sub>3</sub>@CoFe<sub>2</sub>O<sub>4</sub> nanocomposite in peroxy-monosulfate activation for norfloxacin removal. *New J. Chem.* **2020**, *44*, 4185–4198. [[CrossRef](#)]
2. Sisi, J.A.; Fathinia, M.; Khataee, A.; Orooji, Y. Systematic activation of potassium peroxydisulfate with ZIF-8 via sono-assisted catalytic process: Mechanism and ecotoxicological analysis. *J. Mol. Liq.* **2020**, *308*, 113018. [[CrossRef](#)]
3. Bailar, J.C.; Jolly, W.L. *Preparative Inorganic Reactions*; Wiley Interscience: New York, NY, USA, 1964; Volume 1, pp. 1–25.
4. Batten, S.R.; Champness, N.R.; Chen, X.-M.; Garcia-Martinez, J.; Kitagawa, S.; Ohstrom, L. Coordination polymers, metal-organic frameworks and the need for terminology guidelines. *CrystEngComm* **2012**, *14*, 3001–3004. [[CrossRef](#)]
5. James, S.L. Metal-organic frameworks. *Chem. Soc. Rev.* **2003**, *32*, 276–288. [[CrossRef](#)]
6. O’Keeffe, M.; Yaghi, O.M. Deconstructing the crystal structures of metal-organic frameworks and related materials into their underlying nets. *Chem. Rev.* **2012**, *112*, 675. [[CrossRef](#)]
7. Moulton, B.; Zaworotko, M.J. From Molecules to Crystal Engineering: Supramolecular Isomerism and Polymorphism in Network Solids. *Chem. Rev.* **2001**, *101*, 1629–1658. [[CrossRef](#)] [[PubMed](#)]
8. Carlucci, L.; Ciani, G.; Proserpio, D.M. Polycatenation, polythreading and polyknotting in coordination network Chemistry. *Coord. Chem. Rev.* **2003**, *246*, 247–289. [[CrossRef](#)]
9. Erxleben, A. Structures and properties of Zn(II) coordination polymers. *Coord. Chem. Rev.* **2003**, *246*, 203–228. [[CrossRef](#)]
10. Batten, S.R. Topology of interpenetration. *CrystEngComm* **2001**, *18*, 1. [[CrossRef](#)]
11. Huang, F.-P.; Bian, H.-D.; Yu, Q.; Tian, J.-L.; Liang, H.; Yan, S.-P.; Liao, D.-Z.; Cheng, P. Coordination assemblies of Co II/Ni II/Mn II/Zn II with 1, 1'-biphenyl-2, 2'-dicarboxylic acid and three positional isomeric ligands: Structural diversity and properties. *CrystEngComm* **2011**, *13*, 6538–6548. [[CrossRef](#)]
12. Sun, Q.; Wang, Y.Q.; Cheng, A.L.; Wang, K.; Gao, E.Q. Entangled Metal–Organic Frameworks of m-Phenylenediacrylate Modulated by Bis(pyridyl) Ligands. *Cryst. Growth Des.* **2012**, *12*, 2234–2241.
13. Bai, H.Y.; Yang, J.; Liu, B.; Ma, J.F.; Kan, W.Q.; Liu, Y.Y. Syntheses, structures, and photoluminescence of five silver (I) coordination polymers based on tetrakis(imidazol-1-ylmethyl)methane. *CrystEngComm* **2011**, *13*, 5877–5884. [[CrossRef](#)]
14. Li, G.; Lei, Z.; Wang, Q.M. Luminescent Molecular Ag–S Nanocluster [Ag<sub>62</sub>S<sub>13</sub>(SBU<sup>t</sup>)<sub>32</sub>](BF<sub>4</sub>)<sub>4</sub>. *J. Am. Chem. Soc.* **2010**, *132*, 17678–17679. [[CrossRef](#)] [[PubMed](#)]
15. Lan, Y.Q.; Jiang, H.L.; Li, S.L.; Xu, Q. Mesoporous metal-organic frameworks with size-tunable cages: Selective CO<sub>2</sub> uptake, encapsulation of Ln<sup>3+</sup> cations for luminescence, and column-chromatographic dye separation. *Adv. Mater.* **2011**, *23*, 5015. [[CrossRef](#)] [[PubMed](#)]
16. Scaeteanu, V.G.; Maxim, C.; Badea, M.; Olar, R. Zinc(II) Carboxylate Coordination Polymers with Versatile Applications. *Molecules* **2023**, *28*, 1132. [[CrossRef](#)]
17. Fremont, P.; Adet, N.; Parmentier, J.; Xu, X.; Jacques, B.; Dagorne, S. Cationic organometallic complexes of group 12 metals: A decade of progress toward the quest of novel Lewis acidic catalysts. *Coord. Chem. Rev.* **2022**, *469*, 214647. [[CrossRef](#)]
18. Lu, H.; Gan, L. Catalytic Degradation of Bisphenol A in Water by Poplar Wood Powder Waste Derived Biochar via Peroxymonosulfate Activation. *Catalysts* **2022**, *12*, 1164. [[CrossRef](#)]
19. Ghanbari, F.; Moradi, M. Application of peroxy-monosulfate and its activation methods for degradation of environmental organic pollutants: Review. *Chem. Eng. J.* **2017**, *310*, 41–62. [[CrossRef](#)]
20. Li, B.; Chen, X.; Yu, F.; Yu, W.; Zhang, T.; Sun, D. Luminescent Response of One Anionic Metal–Organic Framework Based on Novel Octa-nuclear Zinc Cluster to Exchanged Cations. *Cryst. Growth Des.* **2014**, *14*, 410–413. [[CrossRef](#)]
21. Li, B.; Dai, X.; Meng, X.; Zhang, T.; Liu, C.; Yu, K. Temperature-controlled synthesis and luminescent properties of two novel coordination polymers modeled by hexa-carboxylate ligand derived from cyclotriphosphazene. *Dalton Trans.* **2013**, *42*, 2588–2593. [[CrossRef](#)]
22. Chen, X.; Dong, H.X.; Peng, H.N.; Hong, L.M.; Luo, D.; Zhuang, G.L.; Ye, Q. Three Cd(II) coordination polymers constructed from a series of multidentate ligands derived from cyclotriphosphazene: Synthesis, structures and luminescence properties. *Cryst. Eng. Comm.* **2018**, *20*, 3535–3542. [[CrossRef](#)]
23. Keyikoglu, R.; Khataee, A.; Orooji, Y.; Kobya, M. Synergistic effect of Fe and Co metals for the enhanced activation of hydrogen peroxide in the heterogeneous electro-Fenton process by Co-doped ZnFe layered double hydroxide. *J. Environ. Chem. Eng.* **2022**, *10*, 108875. [[CrossRef](#)]
24. Li, X.; Fu, L.; Chen, F.; Zhao, S.; Zhu, J.; Yin, C. Application of Heterogeneous Catalytic Ozonation in Wastewater Treatment: An Overview. *Catalysts* **2023**, *13*, 342. [[CrossRef](#)]
25. Ansarian, Z.; Khataee, A.; Oskoui, A.S.; Orooji, Y.; Lin, H. Ultrasound-assisted catalytic activation of peroxydisulfate on Ti<sub>3</sub>GeC<sub>2</sub> MAX phase for efficient removal of hazardous pollutants. *Mater. Today Chem.* **2022**, *24*, 100818. [[CrossRef](#)]

26. Patel, B.P.P.; Murali, V.; Rachuri, Y.; Kureshy, R.I.; Khan, N.H.; Suresh, E. Efficient heterogeneous catalysis by dual ligand Zn(ii)/Cd(ii) MOFs for the Knoevenagel condensation reaction: Adaptable synthetic routes, characterization, crystal structures and luminescence studies. *Inorg. Chem. Front.* **2018**, *5*, 2630–2640.
27. Sutradhar, M.; Barman, T.R.; Alegria, E.C.B.A.; Lapa, H.M.; Guedes da Silva, F.C.; Pombeiro, A.J.L. Cd(ii) coordination compounds as heterogeneous catalysts for microwave-assisted peroxidative oxidation of toluene and 1-phenylethanol. *New J. Chem.* **2020**, *44*, 9163–9171. [[CrossRef](#)]
28. Duan, X.; Sun, H.; Wang, Y.; Kang, J.; Wang, S. N-Doping-Induced Nonradical Reaction on Single-Walled Carbon Nanotubes for Catalytic Phenol Oxidation. *ACS Catal.* **2015**, *5*, 553–559. [[CrossRef](#)]
29. APEX2, version 2014.11-0; Bruker AXS Inc.: Madison, WI, USA, 2014.
30. SAINT, version 8.34A; Bruker AXS Inc.: Madison, WI, USA, 2013.
31. SADABS, version 2014/5; Bruker AXS Inc.: Madison, WI, USA, 2014.
32. Sheldrick, G.M. SHELXT—Integrated space-group and crystal-structure determination. *Acta Crystallogr. Sect. A Found Crystallogr.* **2015**, *A71*, 3–8. [[CrossRef](#)]
33. Sheldrick, G.M. Crystal structure refinement with SHELXL. *Acta Crystallogr. Sect. C Struct. Chem.* **2015**, *71*, 3–8. [[CrossRef](#)]
34. Dolomanov, O.V.; Bourhis, L.J.; Gildea, R.J.; Howard, J.A.K.; Puschmann, H. A Complete Structure Solution, Refinement and Analysis Program. *J. Appl. Cryst.* **2009**, *42*, 339–341. [[CrossRef](#)]
35. Spek, A.L. Platon squeeze: A tool for the calculation of the disordered solvent contribution to the calculated structure factors. *Acta Crystallogr.* **2015**, *C71*, 9–18.
36. Spek, A.L. Structure validation in chemical crystallography. *Acta Crystallogr. Sect. D Biol. Cryst.* **2009**, *65*, 148–155. [[CrossRef](#)] [[PubMed](#)]
37. Macrae, C.F.; Edgington, P.R.; McCabe, P.; Pidcock, E.; Shields, G.P.; Taylor, R.; Towler, M.; Van De Streek, J. Visualization and Analysis of Crystal Structures. *J. Appl. Cryst.* **2006**, *39*, 453–457. [[CrossRef](#)]

**Disclaimer/Publisher’s Note:** The statements, opinions and data contained in all publications are solely those of the individual author(s) and contributor(s) and not of MDPI and/or the editor(s). MDPI and/or the editor(s) disclaim responsibility for any injury to people or property resulting from any ideas, methods, instructions or products referred to in the content.